Appl Phys A (2011) 103:1125–1130
DOI 10.1007/s00339-010-6053-x

Applied Physics A
Materials Science & Processing

Magnetocaloric properties of as-quenched $Ni_{50.4}Mn_{34.9}In_{14.7}$ ferromagnetic shape memory alloy ribbons

J.L. Sánchez Llamazares · C. García · B. Hernando · V.M. Prida · D. Baldomir · D. Serantes · J. González

Received: 9 April 2010 / Accepted: 9 September 2010 / Published online: 7 October 2010

Abstract The temperature dependences of magnetic entropy change and refrigerant capacity have been calculated for a maximum field change of $\Delta H = 30$ kOe in as-quenched ribbons of the ferromagnetic shape memory alloy $Ni_{50.4}Mn_{34.9}In_{14.7}$ around the structural reverse martensitic transformation and magnetic transition of austenite. The ribbons crystallize into a single-phase austenite with the $L2_1$-type crystal structure and Curie point of 284 K. At 262 K austenite starts its transformation into a 10-layered structurally modulated monoclinic martensite. The first- and second-order character of the structural and magnetic transitions was confirmed by the Arrott plot method. Despite the superior absolute value of the maximum magnetic entropy change obtained in the temperature interval where the reverse martensitic transformation occurs ($|\Delta S_M^{max}| = 7.2\,J\,kg^{-1}\,K^{-1}$) with respect to that obtained around the ferromagnetic transition of austenite ($|\Delta S_M^{max}| = 2.6\,J\,kg^{-1}\,K^{-1}$), the large average hysteretic losses due to the effect of the magnetic field on the phase transformation as well as the narrow thermal dependence of the magnetic entropy change make the temperature interval around the ferromagnetic transition of austenite of a higher effective refrigerant capacity ($RC_{eff}^{magn} = 95\,J\,kg^{-1}$ versus $RC_{eff}^{struct} = 60\,J\,kg^{-1}$).

J.L. Sánchez Llamazares (✉)
Instituto Potosino de Investigación Científica y Tecnológica (IPICYT), Camino a la Presa San José 2055, Col. Lomas 4a, San Luis Potosí, S.L.P. 78216, Mexico
e-mail: jose.sanchez@ipicyt.edu.mx

C. García
Department of Materials Science and Engineering, MIT, Massachusetts 02139, USA

B. Hernando · V.M. Prida
Departamento de Física, Facultad de Ciencias, Universidad de Oviedo, Calvo Sotelo s/n, 33007 Oviedo, Spain

D. Baldomir · D. Serantes
Departamento de Física Aplicada, Facultad de Física, Universidade de Santiago de Compostela, Campus Sur s/n, 15782 Santiago de Compostela, Spain

J. González
Departamento Física de Materiales, Facultad de Química, UPV, 1072, 20080 San Sebastián, Spain

1 Introduction

In the last few years, considerable attention has been dedicated to study magnetocaloric properties of Heusler-type ferromagnetic shape memory alloys in the $Ni_{50}Mn_{50-x}In_x$ system [1–8]. Upon cooling, these alloys undergo a first-order martensitic transformation (MT) in a narrow composition range from a cubic ferromagnetic austenite (AST), with the $L2_1$- or B2-type crystal structure and a high spontaneous magnetization [9–11], to a structurally modulated martensite (MST). Depending on the chemical composition, the MT may take place from a ferromagnetic AST to either a non-magnetic [1, 3, 4, 6] or a magnetically ordered MST [3, 5]. The magnetization change ΔM caused by the first-order structural MST-to-AST transition and the second-order magnetic transition of AST causes the occurrence of inverse and conventional magnetocaloric effects (MCEs), respectively. Large peak values of the magnetic entropy change ΔS_M associated with the inverse MCE have been reported in a wide temperature interval including room temperature [1, 3, 4, 6]. The latter is an attractive feature of these magnetocaloric materials, which is related to the high sensitivity to small changes of the average valence electron concentration per atom e/a and Mn–Mn interatomic distances

of the martensitic starting phase transition temperature M_S and Curie temperature of MST T_C^M [6, 9–11]. The study of magnetocaloric properties of these alloys is indeed of significant current scientific and applied interest [12].

To date, the studies of magnetocaloric properties of $Ni_{50}Mn_{50-x}In_x$ alloys have been performed on bulk polycrystalline samples produced by arc melting followed by high temperature thermal homogenization annealing [1–11]. To reach a good phase purity and compositional homogeneity, the alloys must be annealed during several hours under vacuum or a protective atmosphere at temperatures above 1000 K. However, rapid solidification using a melt-spinning technique is an effective one-step processing route to produce single-phase polycrystalline ribbons of these materials in the as-quenched state [13, 14]. Preliminary magnetic and X-ray diffraction studies show that as-quenched ribbons of the Heusler alloy $Ni_{50.4}Mn_{34.9}In_{14.7}$ crystallize into a highly ordered cubic AST with the $L2_1$-type structure (space group $Fm3m$; room-temperature lattice parameter $a = 0.5996(3)$ nm) that with the lowering of temperature (T) transforms into a 10-layered modulated (10 M) monoclinic MST phase (with lattice parameters at 150 K: $a = 0.4366(7)$ nm, $b = 0.5630(7)$ nm, $c = 2.121(8)$ nm, and $\beta = 88.81^{o}$) [14]. Its characteristic $M(T)$ curve in field-cooling (FC) and field-heating (FH) modes measured under a constant applied magnetic field $H = 50$ Oe and 2 K/min of heating and cooling rate (Fig. 1) shows structural and magnetic transition temperatures of $M_S = 262$ K, $M_f = 245$ K, $A_S = 262$ K, $A_f = 270$ K, $T_C^M = 192$ K, and $T_C^A = 284$ K (A_S and A_f designate the austenitic start and finish transition temperatures, respectively, and T_C^A the Curie point of AST). The thermal hysteresis ΔT between the forward and reverse martensitic transformations, determined as A_f–M_S, is 8 K. The present study was designed to investigate the magnetic entropy change as a function of temperature $\Delta S_M(T)$ and refrigerant capacity RC around the reverse MT and ferromagnetic transition of AST for a maximum field change of 30 kOe. The results are comparable to those previously reported for bulk alloys.

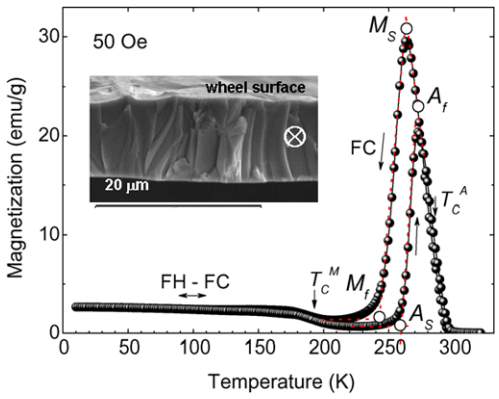

Fig. 1 FH and FC magnetization versus temperature plots under an applied magnetic field of $H = 50$ Oe. The structural and magnetic transitions are indicated in the figure. *Inset*: typical fracture cross-sectional microstructure of ribbons. The *crossed circle symbol* indicates the rolling direction

2 Experimental

Magnetization measurements were performed using a physical property measuring system equipped with a vibrating sample magnetometer module (PPMS-9T, Quantum Design). Measurements were done on a small piece of ribbon of approximately 4 mm in length, 1 mm in width, and around 10 μm in thickness. The inset of Fig. 1 shows a room-temperature SEM image of the typical fractured cross-sectional microstructure of ribbons that are mostly formed by parallel columnar grains with their longer axis perpendicular to both ribbon surfaces. The crossed circle symbol indicates the direction of the major ribbon length (i.e. rolling direction). No phase separation was observed as a further confirmation of the single-phase nature of the samples. The magnetic field was applied along the ribbon length, or rolling direction, to minimize the demagnetizing field effect. $\Delta S_M(T)$ curves were obtained by numerical evaluation of the Maxwell relation $\Delta S_M(T, H) = \mu_0 \int_0^{H_{max}} (\frac{\partial M(H,T)}{\partial T})_{H'} dH'$ [15]. Thus, two sets of isothermal magnetization curves $M(H)$ were measured up to a maximum magnetic field of $H_{max} = 30$ kOe in the temperature intervals 242 K $\leq T \leq$ 270 K and 274 K $\leq T \leq$ 338 K (i.e. where the reverse martensitic transformation and ferromagnetic transition of AST occur, respectively). Different thermal protocols were adopted to reach the measuring temperature T_{measur} in each temperature range. In the reverse martensitic transformation, the isothermal magnetization response of the sample $M(H)$ may be significantly dependent on the thermal history TH followed with the consequent effect on the resulting $\Delta S_M(T)$ curve and the effective or net RC value [8]. To exemplify the significance of the TH for the alloy under study, Fig. 2 shows the field-up and field-down $M(H)$ curves at $T_{measur} = 258$ K (i.e. close to A_S) after reaching this target temperature following three different THs. In TH1 and TH2 the magnetic field strength is set to zero, the sample heated to 330 K (in order to ensure that AST is in paramagnetic state), cooled down to 10 K or 150 K, respectively (a temperature at which the sample is in martensitic state), and then heated to 258 K; in TH3 the sample is first heated in zero field to 330 K and then cooled to 258 K. Note that under TH1 and TH2 the field-up $M(H)$ curves are quite similar and reflect the occurrence of field-induced MST to AST transformation (in practice, both curves overlap up to $H = 50$ kOe). However, for TH3 the sample is a mixture of both phases (i.e. $M_f < 258$ K $< M_S$), and the field only exerts its transformation effect on the

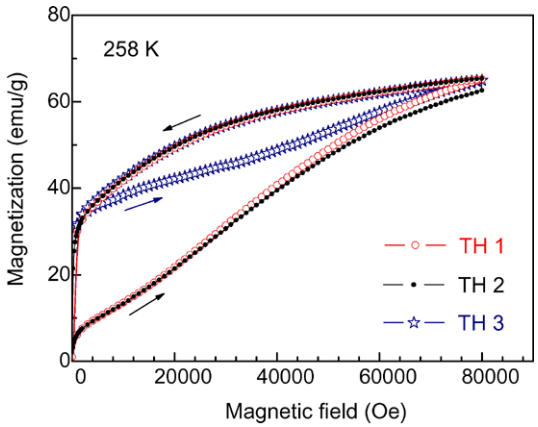

Fig. 2 Field-up and field-down $M(H)$ curves at 258 K measured following three different histories (THs) to reach this measuring temperature (see the text for details)

formed fraction of MST, giving rise to a field-up $M(H)$ curve running above the two other ones. The protocol chosen to study the inverse MCE was TH2; of course, field-down $M(H)$ curves were measured to assess the hysteresis loss as a function of temperature. At temperatures around the magnetic transition of AST a simpler thermal protocol was followed: the field strength is first set to zero, the sample heated to 330 K, and then cooled to the lowest T_{measur} (274 K). After the first $M(H)$ curve is measured the temperature is increased to the next consecutive value and so on. However, as will be described below, above A_f we detected an uncharacteristic little irreversibility between field-up and field-down $M(H)$ curves.

3 Results and discussion

Figure 3a and b show the characteristic isothermal magnetization curves obtained in both temperature ranges. In the temperature range across the reverse martensitic transformation (Fig. 3a), the $M(H)$ curves show a typical field-induced reverse MT. In increasing both the field and the temperature, the low-field region of the field-up curves first shows a high magnetic susceptibility but as the field further increases above H around 2 kOe the magnetization curve continuously rises, showing a large differential susceptibility dM/dH reflecting that a growing fraction of AST progressively forms. The process is irreversible, leading to appreciable hysteretic losses (denoted in the figure by the striped areas). Moreover, it is worth noting that the transformation effect of a magnetic field on MST phase starts at temperatures well below A_S (i.e. notice the irreversible behaviour of field-down $M(H)$ curves from 250 K to $A_S = 262$ K).

The first- and second-order nature of phase transitions was further verified with the help of the Arrott plot method. Figure 4a and b show that well-distinct M^2 versus H/M

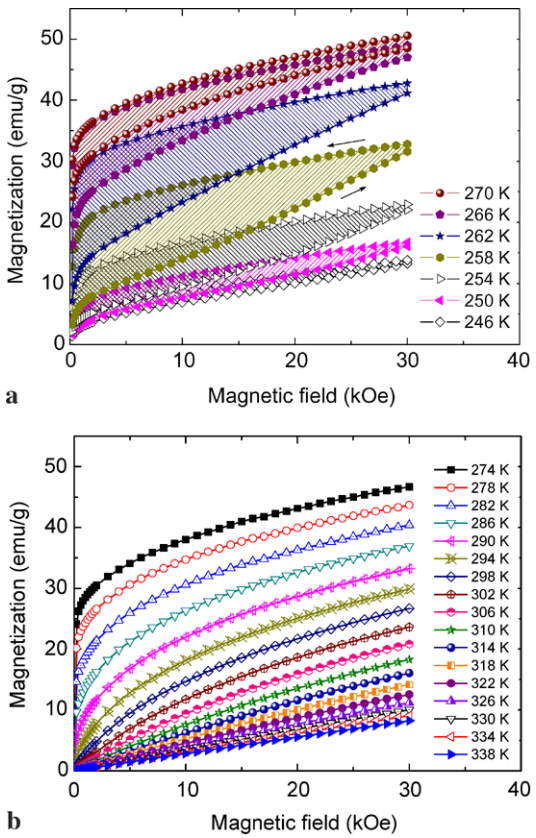

Fig. 3 Isothermal magnetization curves measured across the reverse martensitic transformation (**a**) and magnetic transition of austenite (**b**). The striped areas in (**a**) stand for the hysteretic losses produced by the effect of a magnetic field on the phase transition

plots are obtained in each temperature range. Figure 4a was computed from the $M(H)$ curves measured for $H_{max} = 80$ kOe in order to put better in evidence the S-shape of the plots that is indicative of the first-order nature of the MST to AST transition. In contrast, around T_C^A neither inflection points nor negative slopes are observed, indicating the second-order character of the magnetic phase transition. In the whole temperature range the slope of the plots is positive with a change of sign in their curvature, from negative to positive, around 288 K. The dashed straight line traced serves as an eye guideline to schematically indicate that the Curie point of AST deduced from the graphic is in excellent agreement with the one determined from the low-field $M(T)$ curve.

The $\Delta S_M(T)$ curves at different field values and the field dependence of the absolute value of the maximum magnetic entropy change $|\Delta S_M^{max}(H)|$ are shown in Fig. 5 and its inset, respectively. The $\Delta S_M(T)$ curve at 30 kOe shows a large narrow positive peak located around 258 K, followed by a broader and negative smaller one situated around T_C^A. The height and width of the peaks are in agreement with the first- and second-order nature of the transitions. Whilst at first-order phase transitions an abrupt and large magne-

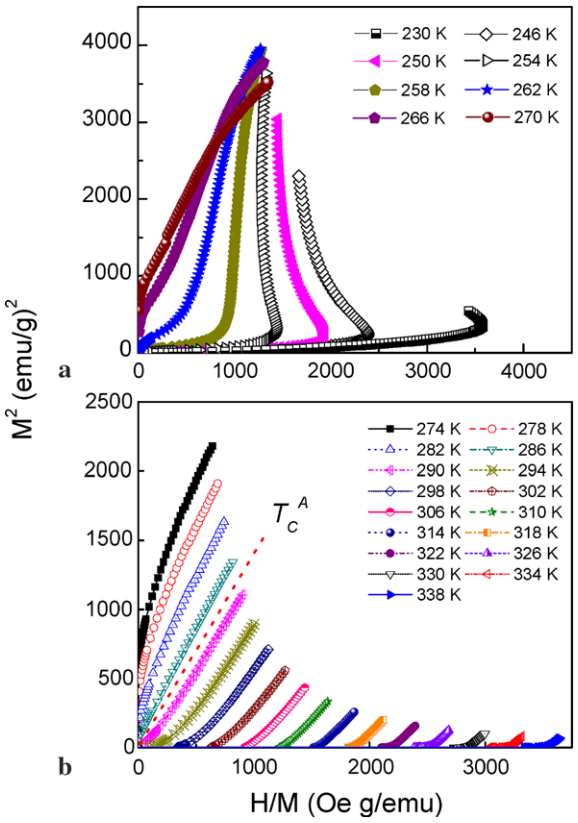

Fig. 4 Arrott plots around the reverse martensitic transformation [(**a**); $H_{max} = 80$ kOe] and magnetic transition of AST [(**b**); $H_{max} = 30$ kOe]. The dashed straight line in (**b**) is an eye guideline to schematically indicate the Curie point of AST

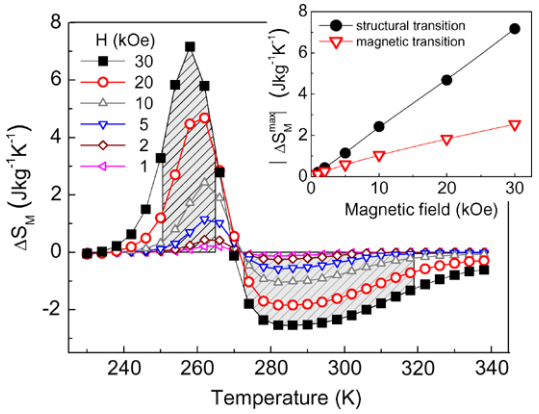

Fig. 5 Temperature dependence of the magnetic entropy change $\Delta S_M(T)$ around the reverse structural transition and magnetic transition of AST at different values of the magnetic field. The *horizontal width of the shaded areas* indicates the useful working temperature interval δT_{FWHM} at 30 kOe, whilst the *inset* shows the field dependence of absolute value of magnetic entropy change ΔS_M^{max} in both temperature intervals

tization change occurs in a very narrow temperature range, at second-order phase transitions it is much more moderate and gradual. $|\Delta S_M^{max}|$ values for the structural and magnetic

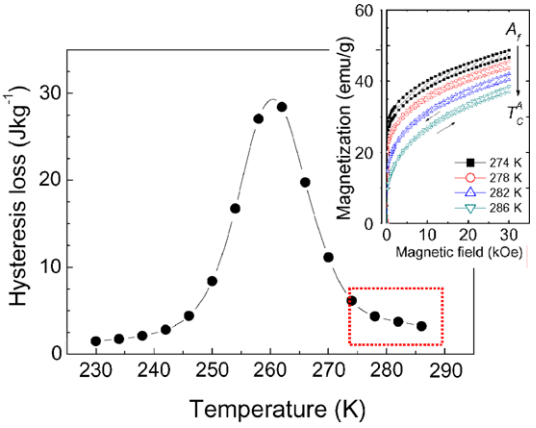

Fig. 6 Hysteretic losses as a function of temperature for a field change of $\Delta H = 30$ kOe owing to the field-induced reverse martensitic transformation. *Inset*: selected field-up and field-down $M(H)$ curves in the temperature interval 274 K $< T <$ 286 K to show the small hysteretic losses detected. The temperature range where this behaviour appears is indicated by the *dashed rectangle traced*

transitions were 7.2 J kg^{-1} K^{-1} and 2.6 J kg^{-1} K^{-1}, respectively. $|\Delta S_M^{max}|$increases approximately proportionally to the magnetic field value H.

To assess the magnetocaloric properties of the material we also computed the refrigerant capacity RC, which estimates the amount of thermal energy that can be transferred by the material between the cold and hot sinks in one ideal thermodynamic cycle. It has been calculated here as $RC = \int_{T_{hot}}^{T_{cold}} [\Delta S_M(T)]_{\Delta H}\, dT$ (i.e. following the method described in [16]). The limits of integration, T_{cold} and T_{hot}, denote the temperatures of the cold and hot sinks which are the temperature values at the full width at half maximum peak (FWHM) of the $\Delta S_M(T)$ curve. Hence, the interval $\delta T_{FWHM} = T_{hot} - T_{cold}$ is also an important attribute of the material as magnetic refrigerant, since it characterizes its useful working temperature range. δT_{FWHM} has a direct effect on the resulting RC value attained. It is the horizontal width of the shaded areas below both peaks of Fig. 5. Notice that the location of the positive $\Delta S_M(T)$ peak has a cutting effect on the left-hand part of the consecutive negative $\Delta S_M(T)$ broad peak associated with the second-order magnetic transition of AST reducing its δT_{FWHM}. The latter is related to the proximity of the first-order structural transition with the second-order magnetic one. For the structural and magnetic transition regions at $\Delta H_{max} = 30$ kOe, we obtained $RC^{struct} = 82$ J kg^{-1} and $RC^{magn} = 99$ J kg^{-1}, respectively. However, to obtain the net or effective value of the refrigerant capacity around the structural transition RC_{eff}^{struct} the average value of hysteretic losses in the temperature range δT_{FWHM} must be subtracted, since they decrease the heat-transfer efficiency of the material during the refrigerant cycle. Figure 6 shows the temperature dependence of hysteretic losses at 30 kOe. The average loss calculated in δT_{FWHM} for the reverse MT was found to be

Table 1 Maximum magnetic entropy change ΔS_M^{max} (absolute value), useful temperature working range ($\delta T_{FWHM} = T_{cold} - T_{hot}$), refrigerant capacity RC, average hysteretic losses, and effective refrigerant capacity RC_{eff} values for $Ni_{50.4}Mn_{34.9}In_{14.7}$ ribbons around the structural and magnetic transitions for a field change of $\Delta H = 30$ kOe

Phase transition	$\lvert\Delta S_M^{max}\rvert$ ($J\,kg^{-1}\,K^{-1}$)	T_{cold} (K)	T_{hot} (K)	δT_{FWHM} (K) ($= T_{hot} - T_{cold}$)	RC ($J\,kg^{-1}$)	Average hysteretic losses ($J\,kg^{-1}$)	RC_{eff} ($J\,kg^{-1}$)
Structural	7.2	251	265	14	82	22	60
Magnetic	2.6	270	315	45	99	4	95

22 $J\,kg^{-1}$ giving rise to $RC_{eff}^{struct} = 60\,J\,kg^{-1}$. On the other hand, during the experiments we realized that small hysteretic losses with a decreasing tendency were unexpectedly observed in this range where AST is the existing phase (i.e. above A_f). The dashed rectangle in the figure indicates the interval where this behaviour was observed. The inset of Fig. 6 shows some of the field-up and field-down $M(H)$ curves measured for $T > A_f$. This phenomenon is currently under study and disappears after a short thermal annealing (800 °C during 10 min, for instance), suggesting that a minor volumetric fraction of the sample undergoes metastability under the presence of the magnetic field above A_f. It is believed that the origin of this phase-instability behaviour lies in the atomic disordering occurring in some regions of the ribbons in austenitic state as a consequence of the non-equilibrium fabrication process used to produce them. When the material is cooled, AST thermally transforms into MST; then the local disorder is transferred to the MST phase that forms in such regions. Above A_f a little fraction of untransformed martensite remains frozen into a major austenitic matrix; therefore, as the temperature increases, or by effect of an increasing magnetic field, this fraction of the material progressively transforms into austenite explaining the behaviour shown by the field-up and field-down isotherms in this temperature range. The average hysteretic loss value estimated in the temperature range δT_{FWHM} related to the magnetic transition is about 4.0 $J\,kg^{-1}$, resulting in $RC_{eff}^{magn} = 95\,J\,kg^{-1}$ (60% higher than RC_{eff}^{struct}). Hence, despite the smaller absolute peak value of the magnetic entropy change achieved around the magnetic transition, RC_{eff}^{magn} is larger than RC_{eff}^{struct}. The latter is explained by both the larger hysteretic losses and the shorter δT_{FWHM} of the reverse martensitic transformation. A summary of the magnetocaloric properties at 30 kOe for the studied ribbons is given in Table 1.

To put our results in a proper context, it is useful is to compare the RC values around both transitions with those reported for bulk alloys with similar values of structural and phase-transition temperatures (calculated by the method given in [16]). However, it must be said that a rigorous comparison is difficult due to the emphatic effect that small compositional shifts may have on the phase-transition temperatures and magnetic properties of $Ni_{50}Mn_{50-x}In_x$ alloys; in addition, the following results correspond to a higher or lower ΔH_{max} value. Pathak et al. [3] reported $RC_{eff}^{struct} = 165\,J\,kg^{-1}$ and $RC^{magn} = 240\,J\,kg^{-1}$ at $\Delta H = 50$ kOe in $Ni_{50}Mn_{34.95}In_{15.05}$ ($A_S \approx 260$ K, $T_C^M \approx 200$ K, and $T_C^A = 328$ K). Sharma et al. [5] obtained $RC_{eff}^{struct} = 72.81\,J\,kg^{-1}$ at $\Delta H = 40$ kOe for $Ni_{50}Mn_{34}In_{16}$ a ($A_S = 225$ K, $T_C^M > A_S$, and $T_C^A = 304$ K). Han et al. [17] found $RC^{struct} = 60\,J\,kg^{-1}$ (non-effective value) for $Ni_{45.5}Mn_{41.5}In_{13}$ ($A_S = 250$ K, $T_C^M = 130$ K, and $T_C^A = 320$ K). Then, the refrigerant capacity of the ribbons produced is something below those of [3], but over the ones reported in [5] and [17].

4 Conclusions

In summary, direct and inverse magnetocaloric properties of $Ni_{50.4}Mn_{34.9}In_{14.7}$ Heusler alloy melt-spun ribbons were evaluated for a maximum field change of 30 kOe. Samples show similar RC values to those reported in the literature for bulk alloys with similar characteristics. The large average hysteretic losses and narrower working temperature interval of the material at the reverse MT transformation considerably reduce RC, leading to a higher refrigeration efficiency around the magnetic transition of austenite. Regardless of the fact that RC values could be improved by properly optimizing the chemical composition and/or performing a thermal annealing (as reported for Heusler alloys in the analogous system Ni–Mn–Sn [18]), is not useless to underline that the preparation method employed is able to produce single-phase austenitic alloys directly from the melt. The efforts for improving their magnetocaloric efficiency in the temperature range of the reverse MT must be addressed to understand the physical mechanisms that may effectively reduce hysteretic losses caused by the field-induced reverse MT.

Acknowledgements This work was partially supported by the research project Nos. MAT2009-13108-C02-01 and MAT2009-08165 (Spanish MICINN) and IB09-13 (FICYT-PA). D. Serantes is grateful to Xunta de Galicia (Maria Barbeito program and Project INCITE 08PXIB236052PR).

References

1. Z.D. Han, D.H. Wang, C.L. Zhang, S.L. Tang, B.X. Gu, Y.W. Du, Appl. Phys. Lett. **89**, 182507 (2006)
2. T. Krenke, E. Duman, M. Acet, E.F. Wassermann, X. Moya, L. Mañosa, A. Planes, E. Suard, B. Ouladdiaf, Phys. Rev. B **75**, 104414 (2007)
3. A.K. Pathak, M. Khan, I. Dubenko, S. Stadler, N. Ali, Appl. Phys. Lett. **90**, 262504 (2007)
4. P.A. Bhobe, K.R. Priolkar, A.K. Nigam, Appl. Phys. Lett. **91**, 242503 (2007)
5. V.K. Sharma, M.K. Chattopadhyay, S.B. Roy, J. Phys. D: Appl. Phys. **40**, 1869 (2007)
6. Z.D. Han, D.H. Wang, C.L. Zhang, H.C. Xuan, J.R. Zhang, B.X. Gu, Y.W. Du, Solid State Commun. **146**, 124 (2008)
7. X. Moya, L. Mañosa, A. Planes, S. Askoy, M. Acet, E.F. Wassermann, T. Krenke, Phys. Rev. B **75**, 184412 (2007)
8. M.K. Chattopadhyay, V.K. Sharma, S.B. Roy, Appl. Phys. Lett. **92**, 022503 (2008)
9. Y. Sutuo, Y. Imano, N. Koeda, T. Omori, R. Kainuma, K. Ishida, K. Oikawa, Appl. Phys. Lett. **85**, 4358 (2004)
10. T. Krenke, M. Acet, E.F. Wassermann, X. Moya, L. Mañosa, A. Planes, Phys. Rev. B **73**, 174413 (2006)
11. T. Kanomata, T. Yasuda, S. Sasaki, H. Nishihara, R. Kainuma, W. Ito, K. Oikawa, K. Ishida, K.-U. Neumann, K.R.A. Ziebeck, J. Magn. Magn. Mater. **321**, 773 (2008)
12. A. Planes, L. Mañosa, M. Acet, J. Phys.: Condens. Matter **21**, 233201 (2009)
13. J.F. Liu, N. Scheerbaum, D. Hinz, O. Gutfleisch, Appl. Phys. Lett. **92**, 162509 (2008)
14. J.L. Sánchez Llamazares, B. Hernando, C. García, J. Gonzalez, L. Escoda, J.J. Suñol, J. Phys. D: Appl. Phys. **42**, 045002 (2009)
15. A.M. Tishin, Y.I. Spichkin, *The Magnetocaloric Effect and Its Applications* (Institute of Physics, Bristol, 2003)
16. K.A. Gschneidner Jr., V.K. Pecharsky, A.O. Pecharsky, C.B. Zimm, Mater. Sci. Forum **315–317**, 69 (1999)
17. Z.D. Han, D.H. Wang, C.L. Zhang, S.L. Tang, B.X. Gu, Y.W. Du, Appl. Phys. Lett. **89**, 182507 (2006)
18. H.C. Xuan, K.X. Xie, D.H. Wang, Z.D. Han, C.L. Zhang, B.X. Gu, Y.W. Du, Appl. Phys. Lett. **92**, 242506 (2008)